THE JOURNAL OF PHYSICAL CHEMISTRY A

Article

pubs.acs.org/JPCA

Propagating Precipitation Waves: Experiments and Modeling

Mark R. Tinsley,* Darrell Collison, and Kenneth Showalter*

C. Eugene Bennett Department of Chemistry, West Virginia University, Morgantown, West Virginia 26506-6045, United States

ABSTRACT: Traveling precipitation waves, including counterrotating spiral waves, are observed in the precipitation reaction of $AlCl_3$ with NaOH [Volford, A.; et al. *Langmuir* **2007**, *23*, 961−964]. Experimental and computational studies are carried out to characterize the wave behavior in cross-section configurations. A modified sol-coagulation model is developed that is based on models of Liesegang band and redissolution systems. The dynamics of the propagating waves is characterized in terms of growth and redissolution of a precipitation feature that travels through a migrating band of colloidal precipitate.

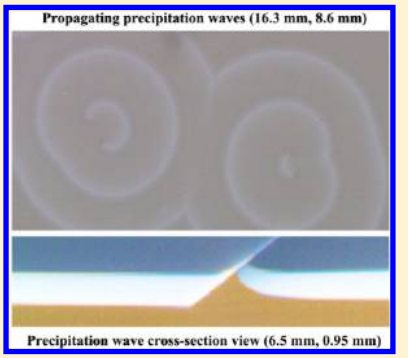

INTRODUCTION

Propagating waves are pervasive in living and nonliving dynamical systems, occurring on a wide range of space and time scales and taking a variety of forms, from electro-mechanical waves in heart tissue[1,2] to spiral waves in propagating flame fronts.[3−5] The mechanism of propagation, generally, is the coupling of a positive feedback process with transport, such as the coupling of autocatalytic chemical reaction with diffusion in the classic example of chemical waves.[6] Physical processes, such as phase changes, may also play a role in propagating waves;[8] for example, surface reconstruction is an essential process in the wave dynamics of the oxidation of CO on single-crystal Pt.[7] In this paper, we report on studies of propagating waves in precipitation reactions, where the coupling of reaction and diffusion plays an important role; however, our experiments and simulations demonstrate that phase changes and the physical properties of the phases are dominant in the wave propagation.

We first consider several systems that exhibit precipitation patterns, as these patterns are intimately connected to the propagating precipitation waves. Liesegang bands[9] are periodic precipitation patterns formed when a pair of coprecipitate species are allowed to diffusively mix.[10] A typical experiment is conducted with a test tube or graduated cylinder and involves two ionic salts, called the inner and outer electrolytes. The inner electrolyte is dissolved in a hydrogel, such as agar, which is allowed to gel in the tube to minimize convective mixing. When a solution of the outer electrolyte is placed on top of this gel, stationary precipitation bands appear in the gel with characteristic periodicity in both their interband separation distance and time of formation.[11,12]

Other forms of complex precipitation processes have also been studied, such as the formation of stationary cones or helical patterns, which use specific combinations of inner and outer electrolytes.[13−16] For example, a variety of structures have been reported in systems involving electrolyte pairs that produce a nonamphoteric hydroxide precipitate (NAHP), such as $NaOH/AgNO_3$ and $NaOH/CuCl_2$.[14,17]

A redissolution Liesegang system is one in which the diffusing outer electrolyte is capable of forming a soluble complex with the original precipitate. Two types of precipitation bands have been reported in these systems. The first is observed when the electrolyte pair $NH_4OH/CoCl_2$ is used.[18] The precipitate $Co(OH)_2$ is initially formed but is then redissolved when the ammonia complex $Co(NH_3)_6^{2+}$ is formed in excess outer electrolyte. Precipitation bands form at the diffusion front with the same periodicity as in a normal Liesegang system. However, the bands behind the front dissolve in the excess outer electrolyte, giving rise to a series of Liesegang bands that appear to move downward through the gel. The bands do not actually move but are formed at the diffusion front and are dissolved when the outer electrolyte reaches a critical dissolution concentration.

The second type of redissolution behavior is that of a single traveling precipitation band that gradually thickens as it travels downward in the gel medium, for example, in the $NaOH/Cr(NO_3)_3$ system.[19−21] A recent study,[22] using $AlCl_3$ as the inner electrolyte and NaOH as the outer electrolyte, also observed a single traveling precipitation band of amphoteric hydroxide; however, in this system, spatiotemporal patterns were observed within the moving precipitation band. These patterns, when viewed from above, appear much like the spiral waves observed in thin films of Belousov−Zhabotinsky (BZ) solutions[23−25] and in other quasi-2D reaction−diffusion systems.[26] Experiments using vertical gel slabs to obtain cross-section visualizations demonstrated that the waves move within the precipitation band, which is simultaneously moving downward in the gel.[22] The wave propagation involves multiple phases arising from the precipitation and redissolution reactions

Received: September 24, 2013
Revised: November 2, 2013

   dx.doi.org/10.1021/jp4095479 | *J. Phys. Chem. A* XXXX, XXX, XXX−XXX

of the ions Al^{3+} and OH^-, and although these processes are complex, no apparent autocatalysis occurs directly from the reaction kinetics. These factors indicate that the wave propagation in the $NaOH/AlCl_3$ precipitation system is fundamentally different from the familiar reaction−diffusion waves seen, for example, in the BZ reaction.

In this paper, we report on new experimental findings in the $NaOH/AlCl_3$ system and identify structural features important in the precipitation wave propagation. On the basis of these findings, we develop a 2D model capable of describing the qualitative features of the traveling waves in a gel slab configuration. Previous computational studies of redissolution Liesegang systems have led to models that describe the experimentally observed stratum of precipitation bands[27,28] as well as the single moving precipitation band.[19,28] We incorporate approaches used in these studies to develop a modified sol-coagulation model[11,12] capable of describing the single moving band of precipitate. Models that have two states of precipitate have been used to describe spatial structure formation in NAHP systems.[29] Here we develop this approach further by introducing a second form of precipitate with physical properties that differ from the precipitate in the single migrating band. The interaction of this precipitate with the other species in the system yields a model that captures the qualitative features of both the migrating band and the traveling waves within the band that are experimentally observed in the $NaOH/AlCl_3$ system.

EXPERIMENTAL SECTION

Methods. An agar gel mixture is prepared by dissolving 1.0 g of agar in 100 mL of distilled water. The solution is heated and stirred until the mixture reaches a temperature of 90.0 °C. The mixture is stirred for an additional 10 min without heating. Powdered aluminum chloride hexahydrate is added to the mixture and stirred until it is fully dissolved. Experiments are carried out using either a gel disk or gel slab configuration. In the former, the gel mixture is poured into a Petri dish (45 mm radius) and allowed to set and return to room temperature. Sodium hydroxide solution is then poured on top of the gel. Gel slab experiments are carried out similarly, but now the gel mixture is poured into a container constructed from two glass slides (50 mm × 75 mm), positioned 1.0 mm apart with a spacer. Images of the gel disk in the Petri dish and the gel slab in the vertical container are taken from above and from the side, respectively. In both cases, back-illumination is utilized (unless otherwise noted). The gel disk allows visualization of the spiral waves, whereas the gel slab configuration offers a cross-section view of the waves propagating within the precipitation band. A variant of the gel slab experiment utilizes a 10 mm separation of the glass slides, allowing simultaneous images from above and from the side to be obtained. This experiment allows the features of the traveling wave to be matched in the above and side views.

Characteristics of the Precipitation Band and Propagating Waves. When the hydroxide solution is added to the top of the gel, a thin band of colloidal precipitate travels downward in the gel, driven by the diffusion of the hydroxide. This band is characterized by a sharp leading edge of precipitate formation and a sharp trailing edge where the precipitate dissolves in the excess hydroxide ion. The chemistry of the system involves the amphoteric properties of $Al(OH)_3$, with this species first forming as a precipitate and then forming the soluble complex ion $Al(OH)_4^-$ in excess hydroxide.[22]

$$Al^{3+}(aq) + 3OH^-(aq) \rightarrow Al(OH)_3(s)$$

$$Al(OH)_3(s) + OH^-(aq) \rightarrow Al(OH)_4^-(aq)$$

The sharp leading and trailing edges of the precipitation band indicate that the reaction kinetics of precipitation and dissolution is fast compared to diffusion within the gel. This behavior of the precipitation band is not unexpected. What is unexpected is the remarkable wave activity that occurs within the precipitation band. The waves propagate outward from spontaneously formed spiral tips through the horizontal plane of the precipitation band. Details of the wave structure are illustrated in Figure 1. Counterrotating spiral waves surrounded by expanding quasi-circular waves are shown in Figure 1a. Figure 1b shows simultaneous top and side images of a wave in a 10 mm gel slab, where the top image shows the wave from

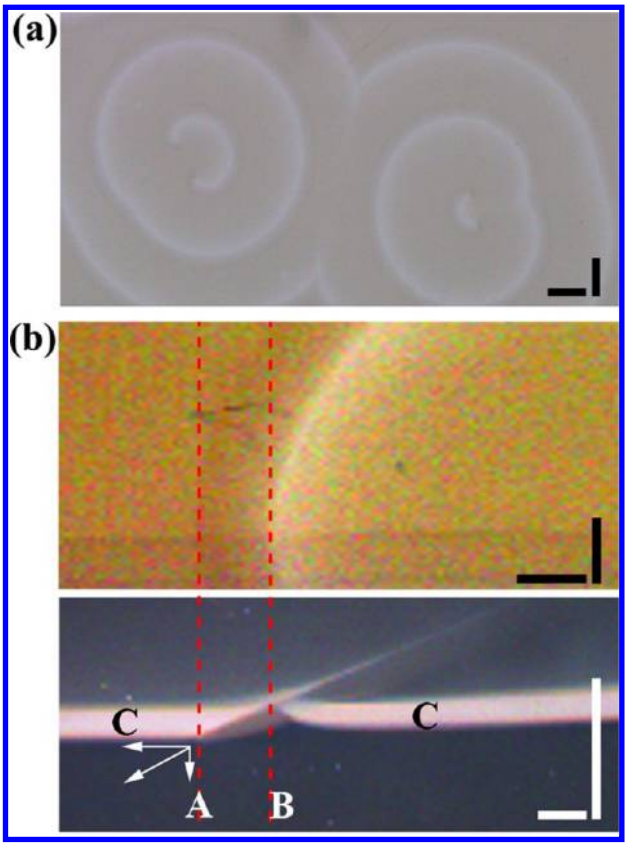

Figure 1. (a) Image, taken from above, of waves in a gel disk within a Petri dish. (b) Simultaneous images taken from above and from the side of a wave in a 10.0 mm slab configuration. The bottom image is taken with front illumination. The structural features, the wavefront **A** and the waveback **B**, are indicated, as well as the migrating precipitation band **C**. Arrows in the bottom panel near the wavefront show relative horizontal and vertical wave velocities and the vector sum showing the overall wave velocity of 5.76×10^{-3} mm s^{-1}. Experimental conditions: (a) A 20.0 mL solution of 2.5 M NaOH is poured on top of 25.0 mL of gelled agar mixture. The agar mixture contains 6.5 g of $AlCl_3$ per 100.0 mL of deionized water and 1.0 g of agar. (b) A 10.0 mL solution of 2.5 M NaOH is poured on top of 15.0 mL of gelled agar mixture with the same composition as in (a). Images are taken at 725 s (a) and 2100 s (b). In the bottom image of (b), the surface of the precipitation feature can be discerned below the diagonal feature in the foreground, which is visible because the wave curves to the right, as shown in the top image of (b). Vertical and horizontal scale bars in (a) and (b) are 1.0 mm.

dx.doi.org/10.1021/jp4095479 | J. Phys. Chem. A XXXX, XXX, XXX−XXX

above the slab and the bottom image shows the side view of the same wave. A diagonal precipitation feature associated with the wave, which plays an essential role in the wave dynamics, is shown in the side-view image. We characterize the wave propagation within the precipitation band in terms of this diagonal feature, with a wavefront and a waveback, which are indicated in Figure 1b. The wavefront exists at the leading edge of the horizontal precipitation band and, in the cross-section side view, appears as the tip of the diagonal precipitation feature. As shown in Figure 1b (bottom), the wavefront leaves a thin line of precipitate to form the diagonal feature. In a 3D representation, the diagonal feature is a surface and the wavefront is the leading edge of this surface. The wavefront can be seen in the above-view image, Figure 1b (top), as the leading edge of a dark region ahead of the more visible light region of the wave. The waveback consists of a concave region of newly formed colloidal precipitate, which connects to the diagonal thin line of precipitate. The waveback precipitate has the same appearance and dissolution properties as the precipitation band; hence, it can be viewed as the reestablishment of the precipitation band following the disturbance by the traveling precipitation wave.

Matching the features of the precipitation wave in the above- and side-view images in Figure 1b (see red vertical dashed lines) shows that the light region in the above-view image is associated with the waveback. The colloidal precipitate visually appears less dense in the waveback than in other regions of the precipitation band, which apparently allows the greater transmitted light intensity. The dark region of the wave in the above-view image matches with the diagonal precipitation feature in the side-view image, and the leading edge matches with the tip of the diagonal feature, the wavefront.

The dynamics of a propagating wave in a gel slab is illustrated in Figure 2a, with three images of the wave taken at successive times. The wavefront propagates at an angle of approximately 22° with respect to the leading edge of the horizontal precipitation band. As can be seen in the images, this angle is effectively constant, indicating that the ratio of the horizontal to vertical components of the wave velocity is constant. The precipitation band broadens and its velocity decreases as it propagates downward in the gel, which is accompanied by a decrease in velocity of the precipitation wave. The essentially constant ratio of the horizontal to vertical velocities reflects the strongly coupled dynamics of the propagating waves and the precipitation band. As the features of the precipitation band change as a function of time, some aspects of the precipitation wave also vary. For example, waves formed early in the experiment exhibit only a small extension of the precipitation feature beyond the waveback. This region lengthens to form an extended precipitation feature as the precipitation band descends in the gel.

Figure 2b shows a side-view image of a wave in which the pH indicator bromothymol blue was added to the gel. The image shows the solution to be basic above and acidic below the precipitation band, as is expected. The low pH immediately below the diagonal precipitation feature between the wavefront and the waveback indicates that the thin line of precipitate acts as a barrier to the diffusion of OH^-. The characteristics of the precipitation feature in this system are similar to those of the passive barriers observed in studies of NAHP systems.[30] Such barriers have been found to behave as ion-selective membranes, restricting diffusion of the outer and inner electrolytes. These studies have also shown that the pH within the passive barrier is high, which indicates that although OH^- is not able to cross the barrier, it is able to diffuse into the barrier.

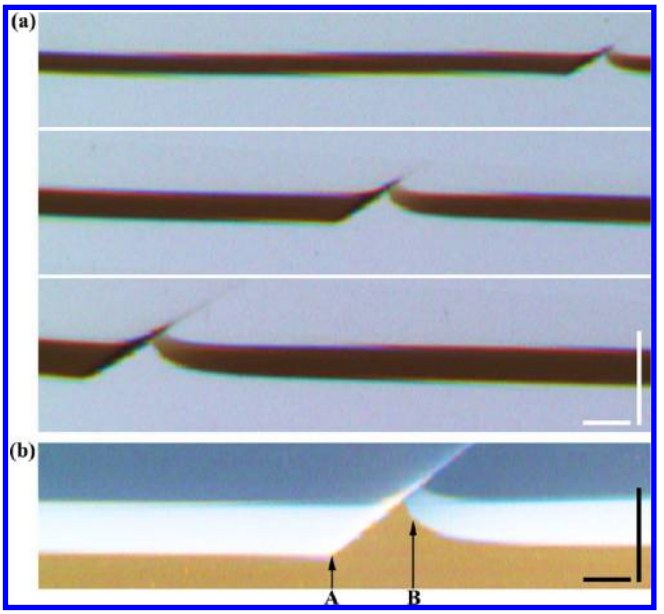

Figure 2. (a) Images showing the spatiotemporal development of a wave in a 1.0 mm gel slab at 375, 1050, and 2050 s. (b) Image of a wave traveling in a gel containing the pH indicator bromothymol blue (with front illumination). The wave structure is labeled to indicate the wavefront **A** and waveback **B**. Experimental conditions: A 1.0 mL solution of 2.5 M NaOH is added to the top of 2.0 mL of gelled agar mixture. The agar mixture contains 6.5 g of $AlCl_3$ per 100.0 mL of deionized water and 1.0 g of agar. Vertical and horizontal scale bars in (a) and (b) are 0.5 mm.

SPATIOTEMPORAL MODEL

Precipitation Band. A model that captures the spatiotemporal dynamics of the $NaOH/AlCl_3$ system should describe both the migrating precipitation band as well as the traveling waves within the band. In this section, we address the first of these requirements using a modified sol-coagulation model of Liesegang band formation. A number of approaches for modeling Liesegang band behavior have been developed,[11,31] and many use a diffusive intermediate, or sol, combined with a threshold above which a precipitate can form and growth can occur.[31] A characteristic feature of these models is the autocatalytic production of the final precipitate, once an intermediate or "smaller" type of precipitate has formed. This autocatalysis leads to a local decrease in the intermediate, and precipitate growth does not occur in the adjacent regions, thus giving rise to successive stationary precipitation bands. An example of such an approach is the CPM model,[32,33] which uses three principal components: sol, small precipitate and large precipitate. The sol is allowed to diffuse, but the two types of precipitate are assumed to be stationary. The sol is continuously formed in the system through reaction of the inner and outer electrolytes.

A modified CPM model allows for the dissolution of both types of precipitate through direct reaction with the outer electrolyte to form a soluble product.[28] This model can account for the experimental observations in redissolution Liesegang systems, such as a stratum of Liesegang bands forming and dissolving, or a single band of precipitate that moves down through the gel.[28]

dx.doi.org/10.1021/jp4095479 | J. Phys. Chem. A XXXX, XXX, XXX–XXX

We apply an approach similar to the sol-coagulation model of Liesagang band formation[11,12] by introducing dissolution of the precipitate and sol components in our description of the $NaOH/AlCl_3$ system,

$$A + B \rightarrow C \quad (1)$$

$$C \rightarrow P_1 \quad (2)$$

$$C + B \rightarrow \quad (3)$$

$$P_1 + B \rightarrow \quad (4)$$

where A, B, C, and P_1 represent the inner electrolyte, outer electrolyte, sol and precipitate, with concentrations a, b, c, and p_1, respectively. The species A, B, and C are free to diffuse with equal diffusion coefficients D. The rates of the four processes are given by k_1ab, $k_2(c - c^*)H(c - c^*)$, k_3cb, and k_4p_1b, respectively. The step function $H(s)$ is defined as $H(s) = 1$ for $s > 0$ and $H(s) = 0$ for $s \leq 0$. The concentration c^* is the threshold value at which coagulation occurs. This model produces a single moving band of precipitate, migrating downward through the medium, much like the redissolution Liesegang experiments.

Propagating Precipitation Waves. The second component of the model involves the dynamics of the wave structures within the precipitation band. As described above, experimental observations show that the diagonal feature plays an essential role in the dynamics of the propagating wave. This precipitate is continuously formed at the wavefront, moving diagonally through the gel, with both horizontal and vertical velocity components. The resultant narrow region of precipitate dissolves slowly along its length, as it is exposed to the downward diffusion of hydroxide ion. The preferential growth in the vicinity of the wavefront and the slow dissolution is convincing evidence that this precipitate is of a different physical form than that in the colloidal precipitation band. It also has a different visual appearance, as is evident in Figures 1 and 2. We label this precipitate P_2, with concentration p_2.

The formation of the thin region of P_2 precipitate involves preferential directional growth, which has been seen in the formation of needle crystals and dendritic structures in supersaturated solutions and undercooled melts.[34] Microscopic models of directional growth, involving front curvature and surface energy considerations, are well developed.[35,36] For the purpose of developing a model of the overall spatiotemporal behavior of the $NaOH/AlCl_3$ system, we construct, instead, a mesoscopic representation of the wavefront growth and movement. Each precipitation wave has an active wavefront at which P_2 growth occurs, and this growth moves the wavefront forward along its diagonal trajectory and leaves behind the thin region of P_2 precipitate.

A wave is initiated in the 2D model simulations of the cross-section representation by switching on P_2 formation at an arbitrary point in the leading edge of the precipitation band. This location constitutes the initial position of the wavefront and is typically chosen to be near the system boundary to allow the largest distance of propagation. The growth of P_2 at the wavefront is then governed by a process analogous to process 2 but with C directly producing P_2, rather than P_1,

$$C \rightarrow P_2 \quad (5)$$

at rate $k_5H(c - c^*)$. The directed growth of the P_2 precipitation feature is modeled as the growth of a solid from the available sol C. In the discretized two-dimensional medium, the diffusing species A, B, and C are described by reaction−diffusion equations with a discrete approximation of the Laplacian operator. The wavefront or tip of the P_2 precipitation feature, however, grows as a solid into a neighboring grid point that is determined by the highest concentration c of sol. The wavefront advances as p_2 at a particular point exceeds the threshold p_2^*. Equation 5 requires that $c > c^*$ at any grid point into which the wavefront grows, as the sol must be above a critical concentration for P_2 growth. A further requirement is that p_1 must be below the threshold p_1^*. Hence, in this scheme, the two types of precipitate compete for the sol, with P_2 formation preferred when p_1 is small. Growth is restricted to the wavefront or tip, and when more than one neighboring point satisfies the conditions for growth, the wavefront grows into the point with the largest sol concentration c.

The formation of P_2 occurs only at the wavefront, and the growth of the wavefront gives rise to the thin diagonal line of precipitate. The precipitate P_2 is subject to dissolution in the presence of downward diffusion of hydroxide ion in a process analogous to reaction 4,

$$P_2 + B \rightarrow \quad (6)$$

at rate k_6bp_2. On the basis of the different physical properties of the precipitate P_2, the diffusion of the inner electrolyte Al^{3+} and the sol does not occur into or out of this narrow region when the concentration of P_2 is above a permeability threshold ($p_2 > p_{2,\mathrm{perm}}$).

The absence of P_1 formation below the line of P_2 precipitate indicates that it serves as a barrier to the downward diffusion of hydroxide ion; therefore, diffusion *across* the precipitation feature does not occur when P_2 is above the threshold concentration $p_{2,\mathrm{perm}}$. However, the eventual dissolution of the P_2 precipitate requires the presence of hydroxide ion, and therefore, it must be able to diffuse *into* the thin line of precipitate. The dissolution of P_2 eventually leads to the line of precipitate becoming permeable, and all species undergo diffusion across this feature once p_2 has become sufficiently small ($p_2 \leq p_{2,\mathrm{perm}}$).

Two-dimensional simulations of the spatiotemporal behavior are carried out using processes 1−6 with diffusion terms. The integration for width X and height Z utilizes no-flux boundary conditions for all species apart from the fixed (Dirichlet) boundary condition for the outer electrolyte, $b(t,x,0) = b_0$, $\forall$ x and $\forall$ t. Initial conditions are given by $c(0,x,z) = 0$, $p_1(0,x,z) = 0$, $\forall$ z and $\forall$ x; $b(0,x,z) = b_0$, $a(0,x,z) = 0$, $\forall$ x and $0 < z < Z_I$; $b(0,x,z) = 0$, $a(0,x,z) = a_0$, $\forall$ x and $Z_I \leq z \leq Z$, where Z_I is the location of the liquid-gel interface.

MODELING RESULTS

Figure 3a shows images of the P_1 precipitation band and the propagating P_2 wave at successive time intervals. The migrating precipitation band can be seen on the left in the top image; on the right, a recently initiated P_2 wave is beginning to grow and propagate. The successive images show the progress of the wave and its impact on the precipitation band. The impermeable region of the P_2 precipitation feature is shown by the filled circles, whereas the permeable region is shown by the open circles. In the second image, in the tail of the wave, p_2 has decreased sufficiently from the dissolution that diffusion of hydroxide ion across the P_2 feature occurs, and a new P_1 precipitation band begins to form on the right. The new precipitation band connects to the underside of the line of P_2 precipitate. A small region of the P_2 feature can be seen behind

dx.doi.org/10.1021/jp4095479 | J. Phys. Chem. A XXXX, XXX, XXX−XXX

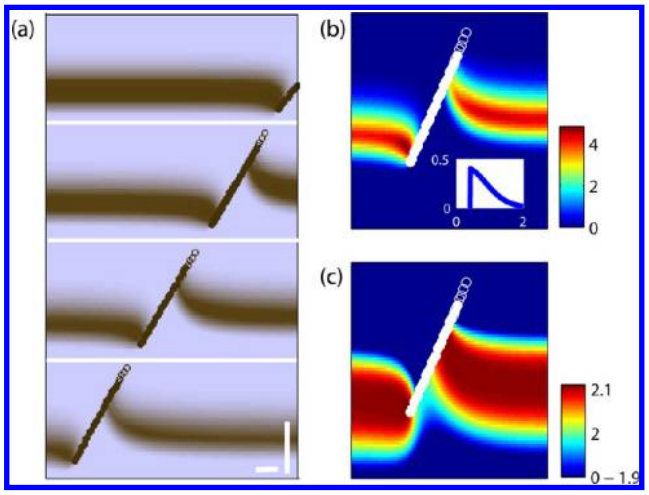

Figure 3. (a) Simulations of the P_1 precipitation band and the P_2 precipitate wave at times 3.78×10^5, 6.58×10^5, 1.03×10^6, and 1.47×10^6. (b) Detail of the wave structure in p_1 at time 6.58×10^5. Inset: p_2 in a point within the diagonal precipitation feature as a function of time (where times are multiplied by 10^5). This curve also approximately corresponds to the spatial profile of p_2 from the wavefront through the waveback along the line of P_2 precipitate. (c) Detail of the wave structure in c at time 6.58×10^5. In each image, grid points with $p_2 > p_{2,\mathrm{perm}}$ are indicated with filled circles; grid points with $p_2 \leq p_{2,\mathrm{perm}}$ are indicated with open circles. Model parameters: $k_1 = 10^{-3}$, $k_2 = 0.02$, $k_3 = 2.5 \times 10^{-6}$, $k_4 = 2.5 \times 10^{-5}$, $k_5 = 2.0 \times 10^{-3}$, $k_6 = 2.5 \times 10^{-5}$, $c^* = 2.1$, $p_1^* = 1.2$, $p_2^* = 0.4$, $p_{2,\mathrm{perm}} = 0.01$. The simulation utilized 400×1000 grid points, with $dx = 6.3$, $dt = 5.0$, $Z_1 = 200$, $a_0 = 10$, $b_0 = 100$, and $D = 1.0$. Vertical and horizontal scale bars in (a) are 20 grid points. Time, distance, and concentration are dimensionless in the nondimensional model 1−6.

the waveback through which diffusion is still prohibited. Much like the experimental behavior, the wavefront travels at essentially the same angle with respect to the precipitation band (~31°), indicating that the ratio of its horizontal and vertical velocity components is virtually constant. However, the velocities of both the precipitation band and the traveling waves within the band decrease as the band migrates downward in the gel.

A more detailed image of the P_1 precipitation band and P_2 wave is shown in Figure 3b, with p_1 indicated in a concentration map. Figure 3c shows the same precipitation band and wave but with the concentration of the sol c. In the absence of P_2, hydroxide ion diffuses freely downward in the medium. The sol concentration rises and coagulates to form P_1, once $c > c^*$. Dissolution of P_1 follows, with increasing hydroxide ion concentration, resulting in a band of P_1 that propagates by diffusion downward through the medium. The sol concentration is higher near the wavefront at the leading edge of the precipitation band. When $c > c^*$, which first occurs immediately ahead of the precipitation band, P_2 growth occurs by process 5, and the wavefront moves ahead into regions of low p_1 and high sol. Figure 3b (inset) shows a time series plot of p_2 at a point which the wavefront grows through and leaves behind in the line of P_2 precipitate. There is an initial sharp rise due to process 5, and the influx of B, due to diffusion, leads to the slow dissolution of P_2 along the line of precipitate. Figure 3b also shows an increased concentration of P_1 in the vicinity of the wavefront. The inability of the sol to diffuse through the line of P_2 precipitate leads to an increase in the production of P_1, because there is a buildup of c in this region.

An interesting emergent feature of the model is the selection of the direction of wave propagation and the angle of the diagonal precipitation feature. Analysis of Figure 3c shows that the sol concentration c is lower to the right of the wavefront and higher to the left due to the restricted diffusion of B across the line of P_2 precipitate. Thus, once the direction of the wavefront motion is selected, it is maintained by this concentration difference, because there is preferential wavefront propagation into regions of higher sol concentration. The magnitude of the propagation angle is related to the threshold values p_1^* and c^*. For example, a lower value of p_1^* tends to increase the horizontal component of the wavefront velocity and thus decrease the angle of propagation with respect to the precipitation band.

The restricted diffusion, due of the presence of the thin region of P_2, prevents the formation of sol C and precipitate P_1 below the region, as shown in Figure 3b,c. Outer electrolyte B increases on the upper side of the diagonal P_2 feature, and when p_2 decreases sufficiently to allow diffusion, the waveback rapidly forms. The presence of a steep gradient in B in this vicinity causes the reconnection of the P_1 precipitation band to the underside of the line of P_2 precipitate, in a region where diffusion across the feature does not occur. The diffusion of B, therefore, has both vertical and horizontal components, as shown by the concaved waveback reconnecting to the diagonal P_2 feature. The precipitation band is slightly offset vertically, in both the experiments and simulations, relative to the band ahead of the wave. However, the band approaches the same vertical level further behind the traveling wave.

More complex behavior observed in the experimental system can also be described by the model. Much like the waves in excitable reaction−diffusion systems, such as the BZ reaction,[23−25] the propagating precipitation waves annihilate on collision. An example of the behavior is shown in Figure 4a, where left and right propagating waves collide, leaving a characteristic V-shaped region in the precipitation band. This

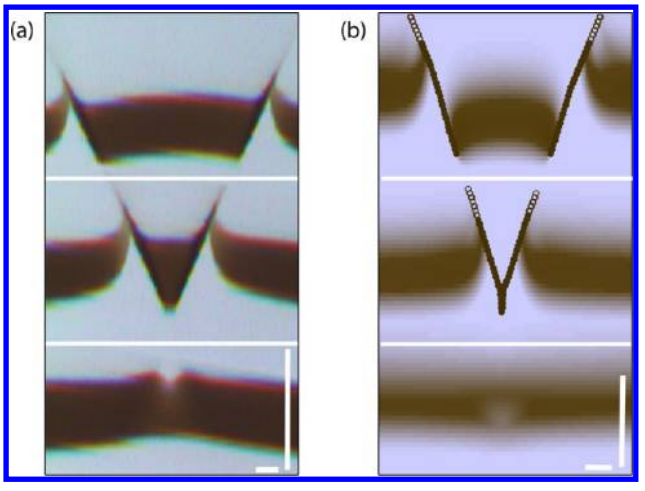

Figure 4. (a) Successive images showing two precipitation waves colliding and subsequently annihilating. Images taken at times 875, 1650, and 2350 s; the experimental conditions are the same as in Figure 2b. (b) Model simulation of colliding and annihilating precipitation waves. Two waves are started at the same time at the left and right boundaries. Images are at times 4.55×10^5, 7.00×10^5, and 8.89×10^5; all parameters are as in Figure 3. Vertical and horizontal scale bars in (a) and (b) are 0.5 mm and 20 grid points, respectively.

dx.doi.org/10.1021/jp4095479 | J. Phys. Chem. A XXXX, XXX, XXX−XXX

feature eventually disappears, giving rise to the appearance of an undisturbed precipitation band.

Figure 4b shows a simulation of two precipitation waves propagating toward each other from the left and right system boundaries. When the wavefronts approach each other and eventually connect, they can no longer advance, as the conditions for wavefront growth no longer exist due to depletion of the sol. The wavebacks then catch up with the respective wavefronts and merge together, with a single, continuous precipitation band emerging, much like the wave collision behavior observed in the experiment.

DISCUSSION

The precipitation waves described here occur through a spontaneous transition in the precipitation process that gives rise to a self-assembling dynamical structure. The physical appearance of the P_2 precipitate is unlike that of the P_1 precipitate, apparently due to a different microstructure, and it acts as a barrier to diffusion. The stationary structures that have been reported in a number of NAHP systems as well as in the $CuCl_2/K_3Fe(CN)_6$ Liesegang system arise through a transition to a secondary precipitation process and have similar features. A major difference between the precipitation waves and the stationary structures is that in the latter case the secondary precipitate does not dissolve to allow the formation of new traveling waves.

The basic wave structure produced by the model is in excellent agreement with the wave profiles observed in experiment. There is essentially no P_1 precipitation band formation below the P_2 feature, from the wavefront to the waveback, due to the restricted diffusion. The waveback displays the same attachment of the P_1 precipitation band to the underside of the P_2 feature, with a similar concave curvature and a slight delay in downward propagation. Although certain details of the shape are sensitive to the model parameters, the basic wave structure is robust and is maintained across a broad range of parameter values.

The mesoscopic model of the traveling precipitation waves is consistent with detailed models for Liesegang and redissolution systems.[27,28,33] A common feature of these systems is autocatalytic growth of the final "large precipitate" in the band formation. In model 1−6, a second form of precipitate is also produced, with the formation and subsequent production of P_2 in process 5. The directed growth of the precipitation feature occurs with the addition of P_2 to the wavefront or tip from the surrounding sol C. Hence, although this growth process requires the presence of P_2, the rate of the process depends only on the concentration c. The P_2 growth takes place at the leading edge of the precipitation band, where the sol concentration is at a maximum, as is observed in experiment.

The model best represents the behavior observed early in an experiment. As the experiment progresses and the precipitation band propagates further downward, there is significantly more P_2 growth, which is clearly visible in the experimental side-view images. This contributes to an increasing length of the P_2 feature. The current model does not describe this variation, because there is a maximum extent of P_2 formation at the wavefront. Inclusion of the conversion of P_1 to P_2, either by direct means or through re-formation of P_1 via C, along with relaxation of the maximum P_2 formation, might allow these features to be captured. The current model also does not describe the increasing thickness of the precipitation band as it moves deeper into the gel. Modifications of the model to better represent this feature may also lead to improvements in the description of the P_2 formation with increasing depth.

An important similarity between propagating precipitation waves and reaction−diffusion waves is that they both can be defined as propagating concentration disturbances. A wavefront develops in the precipitation band by a nucleation process and proceeds to grow, leaving behind the prominent P_2 precipitation feature. The wave advances by directional growth at the wavefront. The recovery of the precipitation band from this disturbance arises from the physicochemical properties of the P_2 feature, which blocks downward diffusion when first formed but then allows diffusion as it undergoes dissolution from the accumulating hydroxide ion. The resumption of downward diffusion of OH^- allows the reestablishment of the P_1 precipitation band, which attaches to the under side of the P_2 precipitation feature, remarkably, in a region where hydroxide ion does not diffusively cross the feature. The overall wave propagation can be viewed as a concentration disturbance propagating through the precipitation band, which is the same ahead and behind the traveling precipitation wave. The concentration disturbance involves the growth and eventual dissolution of the P_2 feature and the disturbance in the P_1 precipitation band.

Though there are similarities between the propagating precipitation waves and reaction−diffusion waves, there are also important differences. Perhaps the most apparent is that the medium, the precipitation band, is itself propagating downward, driven by the diffusion of hydroxide ion. A similar case of a system with a moving medium is the downward propagating flame front in premixed oxygen-butane mixtures, which displays spiral and target waves within the flame front.[3−5] Another important difference is that the constant waveform, constant velocity propagating waves in reaction−diffusion systems are sustained by autocatalysis, whereas the precipitation wavefront grows by process 5, with kinetics dependent on the concentration of sol, which is sustained by the downward diffusion of hydroxide ion. These waves are also not constant waveform, constant velocity waves but exhibit velocities and waveforms that vary with the vertical propagation distance of the precipitation band.

Valuable insights into many types of propagating waves have been obtained from studies of reaction−diffusion waves, from spiral and scroll waves in cardiac tissue[1,2] to spreading depression (depolarization) in the brain.[37] It is apparent, however, that most propagating waves in biological systems involve processes other than the coupling of reaction with diffusion. It seems unlikely that any biological waves involve the processes in the precipitation waves described here; however, the wave propagation mechanism might offer insights into similarly complex waves in biological systems. Directed growth is common in biological systems, and the formation of a substance that impedes diffusive transport seems quite plausible in the complex cytoplasm of living cells.

AUTHOR INFORMATION

Corresponding Authors

*M. R. Tinsley: e-mail, mark.tinsley@mail.wvu.edu.
*K. Showalter: e-mail, kenneth.showalter@mail.wvu.edu.

Notes

The authors declare no competing financial interest.

■ ACKNOWLEDGMENTS

This material is based on work supported by the National Science Foundation (Grant No. CHE-1212558).

■ REFERENCES

(1) Winfree, A. *The Geometry of Biological Time*; Springer: Berlin, 2001.
(2) Murray, J. D. *Mathematical Biology: I. An Introduction (Interdisciplinary Applied Mathematics) (Pt. 1)*; Springer: Berlin, 2007.
(3) Pearlman, H. G.; Ronney, P. D. Self-Organized Spiral and Circular Waves in Premixed Gas Flames. *J. Chem. Phys.* **1994**, *101*, 2632−2633.
(4) Scott, S. K.; Wang, J. C.; Showalter, K. Modelling Studies of Spiral Waves and Target Patterns in Premixed Flames. *J. Chem. Soc., Faraday Trans.* **1997**, *93*, 1733−1739.
(5) Panfilov, V.; Bayliss, A.; Matkowsky, B. J. Spiral Flames. *Appl. Math. Lett.* **2003**, *16*, 131−135.
(6) Cross, M. C.; Hohenberg, P. C. Pattern-Formation Outside of Equilibrium. *Rev. Mod. Phys.* **1993**, *65*, 851−1112.
(7) Mikhailov, A. S.; Showalter, K. Control of Waves, Patterns and Turbulence in Chemical Systems. *Phys. Rep.* **2006**, *425*, 79−194.
(8) Mikhailov, A. S.; Ertl, G. Nonequilibrium Microstructures in Reactive Monolayers as Soft Matter Systems. *ChemPhysChem* **2009**, *10*, 86−100.
(9) Liesegang, R. Uber einige Eigenschaften von Gallerten. *Naturwiss. Wochenschr* **1896**, *11*, 353−362.
(10) Müller, S.; Ross, J. Spatial Structure Formation in Precipitation Reactions. *J. Phys. Chem. A* **2003**, *107*, 7997−8008.
(11) Antal, T.; Droz, M.; Magnin, J.; Rácz, Z.; Zrinyi, M. Derivation of the Matalon-Packter Law for Liesegang Patterns. *J. Chem. Phys.* **1998**, *109*, 9479−9486.
(12) Lagzi, I. Controlling and Engineering Precipitation Patterns. *Langmuir* **2012**, *28*, 3350−3354.
(13) Müller, S. C.; Kai, S.; Ross, J. Curiosities in Periodic Precipitation Patterns. *Science* **1982**, *216*, 635−637.
(14) Hantz, P. Pattern Formation in the NaOH + $CuCl_2$ Reaction. *J. Phys. Chem. B* **2000**, *104*, 4266−4272.
(15) Thomas, S.; Lagzi, I.; Molnár, F., Jr.; Rácz, Z. Probability of the Emergence of Helical Precipitation Patterns in the Wake of Reaction-Diffusion Fronts. *Phys. Rev. Lett.* **2013**, *110*, 078303.
(16) Thomas, S.; Lagzi, I.; Molnár, F., Jr.; Rácz, Z. Helices in the Wake of Precipitation Fronts. *Phys. Rev. E* **2013**, *88*, 022141.
(17) Hantz, P. Regular Microscopic Patterns Produced by Simple Reaction-diffusion Systems. *Phys. Chem. Chem. Phys.* **2002**, *4*, 1262−1267.
(18) Nasreddine, V.; Sultan, R. Propagating Fronts and Chaotic Dynamics in $Co(OH)_2$ Liesegang Systems. *J. Phys. Chem. A* **1999**, *103*, 2934−2940.
(19) Zrinyi, M.; Galfi, L.; Smidroczki, E. Direct Observation of a Crossover from Heterogeneous Traveling Wave to Liesegang Pattern Formation. *J. Phys. Chem.* **1991**, *95*, 1618−1620.
(20) Sultan, R.; Panjarian, S. Propagating Fronts in 2D $Cr(OH)_3$ Precipitate Systems in Gelled Media. *Physica D* **2001**, *157*, 241−250.
(21) Al-Ghoul, M.; Ammar, M.; Al-Kaysi, R. O. Band Propagation, Scaling Laws and Phase Transition in a Precipitate System. I: Experimental Study. *J. Phys. Chem. A* **2012**, *116*, 4427−4437.
(22) Volford, A.; Izsák, F.; Ripszám, M.; Lagzi, I. Pattern Formation and Self-organization in a Simple Precipitation System. *Langmuir* **2007**, *23*, 961−964.
(23) Zaikin, A. N.; Zhabotinsky, A. M. Concentration Wave Propagation in 2-Dimensional Liquid-Phase Self-Oscillating System. *Nature* **1970**, *225*, 535−537.
(24) Field, R.; Körös, E.; Noyes, R. Oscillations in Chemical Systems. II. Thorough Analysis of Temporal Oscillation in the Bromate-Cerium-Malonic Acid System. *J. Am. Chem. Soc.* **1972**, *94*, 8649−8664.
(25) Taylor, A. F. Mechanism and Phenomenology of an Oscillating Chemical Reaction. *Prog. React. Kinet. Mech.* **2002**, *27*, 247−325.
(26) Berenstein, I.; Munuzuri, A. P.; Yang, L. F.; Dolnik, M.; Zhabotinsky, A. M.; Epstein, I. R. Breathing Spiral Waves in the Chlorine Dioxide-Iodine-Malonic Acid Reaction-Diffusion System. *Phys. Rev. E* **2008**, *78*, 025101.
(27) Henisch, H. Liesegang Ring Formation in Gels. *J. Cryst. Growth* **1986**, *76*, 279−289.
(28) Al-Ghoul, M.; Sultan, R. Front Propagation in Patterned Precipitation. 1. Simulation of a Migrating $Co(OH)_2$ Liesegang Pattern. *J. Phys. Chem. A* **2001**, *105*, 8053−8058.
(29) Horvát, S.; Hantz, P. Pattern Formation Induced by Ion-Selective Surfaces: Models and Simulations. *J. Chem. Phys.* **2005**, *123*, 34707.
(30) Hantz, P.; Partridge, J.; Láng, G. Ion-Selective Membranes Involved in Pattern-Forming Processes. *J. Phys. Chem. B* **2004**, *108*, 18135−18139.
(31) Izsák, F.; Lagzi, I. In *Precipitation Patterns in Reaction-Diffusion Systems*; Lagzi, I., Ed.; Research Signpost: Kerala, India, 2010.
(32) Chernavskii, D. S.; Polezhaev, A. A.; Müller, S. C. A Model of Pattern Formation by Precipitation. *Physica D* **1991**, *54*, 160−170.
(33) Polezhaev, A. A.; Müller, S. C. Complexity of Precipitation Patterns: Comparison of Simulation with Experiment. *Chaos* **1994**, *4*, 631−636.
(34) Dougherty, A.; Gollub, J. Steady-State Dendritic Growth of NH_4Br from Solution. *Phys. Rev. A* **1988**, *38*, 3043−3053.
(35) Langer, J. Instabilities and Pattern Formation in Crystal Growth. *Rev. Mod. Phys.* **1980**, *52*, 1−28.
(36) Langer, J. S. Dendrites, Viscous Fingers, and the Theory of Pattern Formation. *Science* **1989**, *243*, 1150−1156.
(37) Dahlem, M. A.; Graf, R.; Strong, A. J.; Dreier, J. P.; Dahlem, Y. A.; Sieber, M.; Hanke, W.; Podoll, K.; Schöll, E. Two-Dimensional Wave Patterns of Spreading Depolarization: Retracting, Re-Entrant, and Stationary Waves. *Physica D* **2010**, *239*, 889−903.